PROCEEDINGS, 44th Workshop on Geothermal Reservoir Engineering
Stanford University, Stanford, California, February 11-13, 2019
SGP-TR-214

The Necessity for Iteration in the Application of Numerical Simulation to EGS: Examples from the EGS Collab Test Bed 1

Mark White[1], Tim Johnson[1], Tim Kneafsey[2], Doug Blankenship[3], Pengcheng Fu[4], Hui Wu[4], Ahmad Ghassemi[5], Jianrong Lu[5], Hai Huang[6], Ghanashyam Neupane[6], Curt Oldenburg[2], Christine Doughty[2], Bud Johnston[7], Philip Winterfeld[8], Ryan Pollyea[9], Richard Jayne[9], Adam Hawkins[10], Yuran Zhang[10], and EGS Collab Team[11]

[1]Energy and Environment Directorate, Pacific Northwest National Laboratory, Richland, WA 99352, USA

[2]Earth and Environmental Sciences, Lawrence Berkeley National Laboratory, Berkeley, CA 94720, USA

[3]Energy Research, Sandia National Laboratory, Albuquerque, NM, 87185, USA

[4]Atmospheric, Earth and Energy Division, Lawrence Livermore National Laboratory, Livermore, CA 94550, USA

[5]Petroleum and Geologic Engineering, The University of Oklahoma, Norman, OK 94550, USA

[6]Energy and Environment Science and Technology Directorate, Idaho National Laboratory, Idaho Falls, ID

[7]Geothermal Technologies Program, National Renewable Energy Laboratory, Golden, CO 80401, USA

[8]Petroleum Engineering, Colorado School of Mines, Golden, CO 80401, USA

[9]Geosciences, Virginia Tech, Blacksburg, VA 24061, USA

[10]TomKat Center for Sustainable Energy, Geothermal Program, Stanford University, Stanford, CA 94305, USA

Email: mark.white@pnnl.gov

Keywords: numerical simulation, EGS Collab, enhanced geothermal systems, Sanford Underground Research Facility, meso-scale experiment, hydraulic fracture, natural fracture, THMC modeling

ABSTRACT

The United States Department of Energy, Geothermal Technologies Office (GTO) is funding a collaborative investigation of enhanced geothermal systems (EGS) processes at the meso-scale. This study, referred to as the EGS Collab project, is a unique opportunity for scientists and engineers to investigate the creation of fracture networks and circulation of fluids across those networks under in-situ stress conditions. The EGS Collab project is envisioned to comprise three experiments and the site for the first experiment is on the 4850' Level in phyllite of the Precambrian Poorman formation, at the Sanford Underground Research Facility, located at the former Homestake Gold Mine, in Lead, South Dakota. Principal objectives of the project are to develop a number of intermediate-scale field sites and to conduct well-controlled in situ experiments focused on rock fracture behavior and permeability enhancement. Data generated during these experiments will be compared against predictions of a suite of computer codes specifically designed to solve problems involving coupled thermal, hydrological, geomechanical, and geochemical processes. Comparisons between experimental and numerical simulation results will provide code developers with direction for improvements and verification of process models, build confidence in the suite of available numerical tools, and ultimately identify critical future development needs for the geothermal modeling community. Moreover, conducting thorough comparisons of models, modelling approaches, measurement approaches and measured data, via the EGS Collab project, will serve to identify techniques that are most likely to succeed at the Frontier Observatory for Research in Geothermal Energy (FORGE), the GTO's flagship EGS research effort. As noted, outcomes from the EGS Collab project experiments will serve as benchmarks for computer code verification, but numerical simulation additionally plays an essential role in designing these meso-scale experiments. This paper reviews specific numerical simulations supporting the design of experiments within Test Bed 1, a volume of phyllite rock under in-situ stress conditions off the western side of the West Access Drift on the 4850 Level, near Governor's Corner. Numerical simulations were executed prior to the start of hydraulic stimulation activities within Test Bed 1 following standard practices, using best estimates of principal stress conditions, thermal conditions, and the rock petrophysical properties, including geomechanical properties. These simulations indicated notching of the borehole would promote the initiation of transverse fractures, seismic magnitudes during the

[11] J. Ajo-Franklin, S.J. Bauer, T. Baumgartner, K. Beckers, D. Blankenship, A. Bonneville, L. Boyd, S. Brown, S.T. Brown, J.A. Burghardt, T. Chen, Y. Chen, K. Condon, P.J. Cook, D. Crandall, P.F. Dobson, T. Doe, C.A. Doughty, D. Elsworth, J. Feldman, A. Foris, L.P. Frash, Z. Frone, P. Fu, K. Gao, A. Ghassemi, H. Gudmundsdottir, Y. Guglielmi, G. Guthrie, B. Haimson, A. Hawkins, J. Heise, M. Horn, R.N. Horne, J. Horner, M. Hu, H. Huang, L. Huang, K.J. Im, M. Ingraham, R.S. Jayne, T.C. Johnson, B. Johnston, S. Karra, K. Kim, D.K. King, T. Kneafsey, H. Knox, J. Knox, D. Kumar, K. Kutun, M. Lee, K. Li, R. Lopez, M. Maceira, P. Mackey, N. Makedonska, C.J. Marone, E. Mattson, M.W. McClure, J. McLennan, T. McLing, C. Medler, R.J. Mellors, E. Metcalfe, J. Miskimins, J. Moore, J.P. Morris, S. Nakagawa, G. Neupane, G. Newman, A. Nieto, C.M. Oldenburg, W. Pan, T. Paronish, R. Pawar, P. Petrov, B. Pietzyk, R. Podgorney, Y. Polsky, J. Popejoy S. Porse, B.Q. Roberts, M. Robertson, W. Roggenthen, J. Rutqvist, D. Rynders, H. Santos-Villalobos, M. Schoenball, P. Schwering, V. Sesetty, C.S. Sherman, A. Singh, M.M. Smith, H. Sone, F.A. Soom, C.E. Strickland, J. Su, D. Templeton, J.N. Thomle, C. Ulrich, N. Uzunlar, A. Vachaparampil, C.A. Valladao, W. Vandermeer, G. Vandine, D. Vardiman, V.R. Vermeul, J.L. Wagoner, H.F. Wang, J. Weers, J. White, M.D. White, P. Winterfeld, T. Wood, S. Workman, H. Wu, Y.S. Wu, Y. Wu, E.C. Yildirim, Y. Zhang, Y.Q. Zhang, J. Zhou, Q. Zhou, M.D. Zoback

hydraulic stimulation would be below 0.1 magnitude on the Richter scale, a rock thermal conductivity of 5.0 W/m K yielded agreement with nearby kISMET borehole temperature logs, back pressure on the production borehole would increase circulation across the test bed, and the production borehole would serve to halt propagation of the hydraulic fracture to the drift. Pre-existing natural fractures, heterogeneities in the rock properties, monitoring boreholes, and overlooked mine elements have prompted a second look at numerically modeling stimulation, fluid circulation, tracer migration, and thermal breakthrough. Numerical simulation is an invaluable tool for providing insight and understanding to complex physical processes. The success of simulations, however, often depends on including all of the salient features of the system in the founding conceptual model. This paper takes a retrospective look at examples where the conceptual model and simulation was sufficient to provide accurate forecasts and those where elements were missing, necessitating rethinking of the simulation.

1. INTRODUCTION

In October 2016, the United States Department of Energy (DOE), Geothermal Technologies Office (GTO) announced a funding opportunity that was to be collaborative in nature and act as a research and development path between laboratory-scale stimulation and rock mechanics studies and the large field scale of the future Frontier Observatory for Research in Geothermal Energy (FORGE) investigations (U.S. Department of Energy, 2017). The recipient of the Collab award was announced in early 2017 to a project led by the Lawrence Berkeley National Laboratory (LBNL), and initially termed the Stimulation Investigations for Geothermal Modeling Analysis and Validation project, whose acronym referred to the symbol used for vertical stress (σ_v). This collaborative project, now known as EGS Collab, involves national laboratories, universities and private industry teaming to conduct stimulation and circulation experiments, and verify computer codes, numerical algorithms and approaches, and process models against the generated data. This three-year project (Kneafsey et al., 2018) has been tasked with providing new knowledge and modeling capabilities, forming a path from laboratory scale to the field scale of FORGE. Each year during this project the Modeling and Simulation Working Group is responsible for reporting on the state of numerical simulators and simulations associated with the project. During the first year of the project, numerical simulations were generally directed at supporting the design of Experiment 1 (White et al., 2017; White et al., 2018). At that time, numerical simulations were being conducted based on characterization data that were available from the kISMET project, which involved five vertical or deviated vertical boreholes, also drilled from the 4850 drift (Oldenberg et al., 2016). Borehole logging at the kISMET site revealed existing natural fracture and foliation features, but did not identify any open natural fractures, which supported the notion of the host rock surrounding the kISMET boreholes as being of low permeability and clear of visible open fractures.

The process of numerical simulation, especially for geologic systems, starts with conceptual models of the critical processes and geologic and engineered settings. The critical processes to be modeled generally define the type of numerical simulator required, and the geologic and engineered settings often define computational domain geometries and parameter distributions. Specific numerical simulator capabilities become factors for complex geologic and engineered settings. For EGS Collab Experiment 1, numerical simulations executed in support of the experimental design were founded on the characterization results of the kISMET project. These data and resulting conceptual models yielded successful forecast in some instances, but in others ignoring natural fractures, fracture heterogeneities, and engineered systems, such as the rock bolting and wire mesh in the drift, necessitated a second go at executing numerical simulations. This paper reviews examples from numerical simulations conducted as part of the EGS Collab project, which were successful in forecasting experimental outcomes and observations, and examples where additional characterization information was incorporated into a simulation, or the simulation approach was modified in response to experimental observations. It is important here to distinguish between a numerical simulator failure and errors in conceptualization of the system to be modeled. Numerical simulators yield approximate solutions to geologic problems, and occasionally have bugs that yield erroneous solutions. Under these situations, iteration in the application of numerical simulation would require code modifications and re-execution of the simulation. The simulators being applied on the EGS Collab project generally are mature computer codes that have been verified through code comparison studies and previous applications, making bug type errors unlikely. For the EGS Collab project, therefore, iteration in the application of numerical simulation arises from the realization that the geologic system differs from the original conceptualization. Under this situation, the numerical simulator executed properly, but the system modeled was not representative of the experimental testbed.

2. OVERVIEW OF EXPERIMENTAL ACTIVITIES

EGS Collab Experiment 1 is being conducted within a volume of predominately phyllite rock on the western side of the 4850 Level (4,850 feet below ground surface) West Access Drift (drift) within Sanford Underground Research Facility (SURF) near the kISMET site (Oldenburg et al., 2016). Eight boreholes were drilled into the experimental volume (Testbed 1); two boreholes designed for flow and six boreholes designed for monitoring (Morris et al., 2018). The flow boreholes (E1-I injection, and E1-P production) were drilled from the drift wall, nominally in the direction of the minimum principal horizontal stress (i.e., σ_h), with the intent of creating a connecting hydraulic fracture between these two boreholes. The flow boreholes were collared near the drift wall, but otherwise open. Four of the monitoring boreholes were drilled subhorizontally parallel to the anticipated hydraulic fracture (E1-PDT, E1-PDB, E1-PST, and E1-PSB) in v-pattern pairs from the drift wall, on either side of the anticipated hydraulic fracture. Two of the monitoring boreholes were drilled in a v-pattern pair from the drift wall in a direction orthogonal to the anticipated hydraulic fracture (E1-OT and E1-OB), midway between the injection and production boreholes. The monitoring boreholes were filled with instrumentation strings (Knox et al., 2017) and grouted with low electrical resistivity grout. The borehole layout is shown in Fig. 1a. The layout of the experimental testbed shown in Fig. 1a evolved from estimations of the stress state and an understanding of the nature of the phyllite rock, from the kISMET project (Oldenburg et al., 2016) and supporting numerical simulations (White et al., 2017; White et al., 2018), which generally assumed the rock mass to be of low permeability with few active natural fractures, but subject to a thermally altered stress field, from drift cooling.

Over the course of the year, a series of experiments were conducted within the testbed, which were either hydraulic stimulation or hydraulic characterization in nature. The hydraulic stimulation experiments were generally shorter in duration and were specifically designed to

hydraulically connect E1-I and E1-P. The hydraulic characterization experiments involved short- and intermediate-term flow tests, tracer tests, and limited thermal tests. To understand the evolution of numerical simulation approaches and conceptual models about the test bed, it is necessary to review the key results from this series of experiments. All boreholes in the experimental volume were core drilled with HQ sized diamond bits, yielding a borehole diameter of 96 mm (3.78 in) and core diameter of 63.5 mm (2.5 in), cores were logged and boxed, and gyro logs were taken to establish borehole trajectories. One of the first experimental results from the test bed occurred during the drilling of E1-P, which occurred after the drilling of E1-OT and E1-OB. When drilling reached a depth of roughly 27 m (90 ft) dripping water was noted out of E1-OT, and when a depth of roughly 36 m (118 ft) had been reached, a steady flow of water was noted from E1-OT, when water was being circulated by the drilling operations. This observation was the first indication of a hydraulically active natural fracture within the test bed, and is referenced as the OT-P connector fracture system. This fracture was identified in the core logs and via a sewer camera log of E1-P. The location and orientation of the OT-P connector are shown in Fig. 1b.

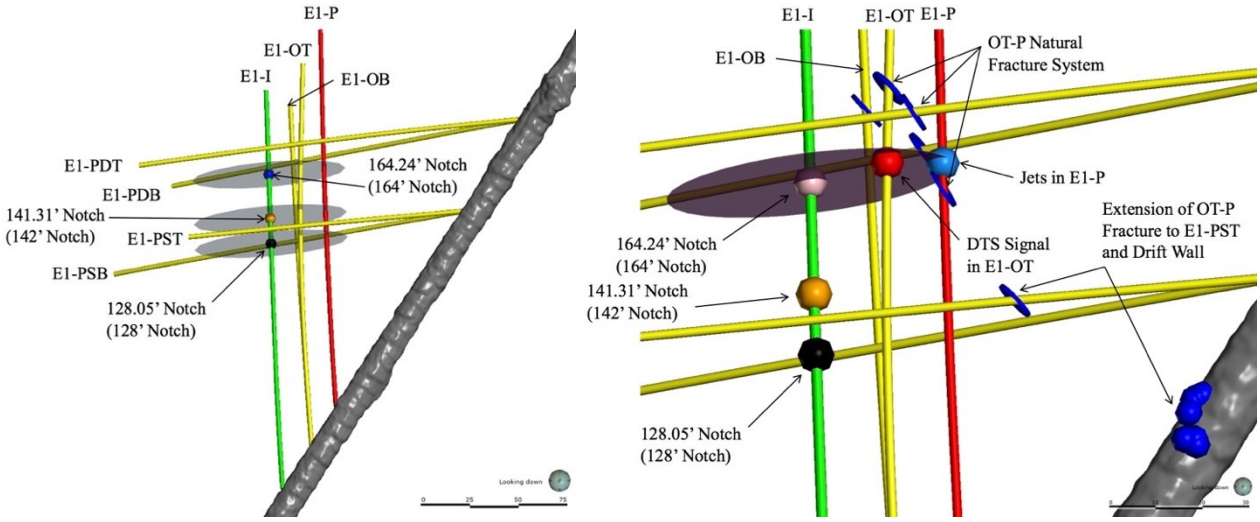

Figure 1: (a) EGS Collab Test Bed 1 borehole locations. Drift shown in grey with shading, and notched locations along E1-I shown as spheres, with corresponding anticipated hydraulic fracture planes shown as translucent grey discs. (b) EGS Collab Test Bed 1 borehole locations and OT-P connector natural fracture system. Images generated with Leapfrog Software.

2.1 Chronologic Order of Experimental Activities

The chronologic order of the key experimental activities is provided for reference in Table 1.

Table 1. Key experimental activities in chronological order.

Experimental Activity	Start Date	End Date
Drilling of E1-OT	Oct. 2, 2017	Oct. 13, 2017
Drilling of E1-OB	Oct. 16, 2017	Oct. 24, 2017
Drilling of E1-P	Oct. 25, 2017	Nov. 2, 2017
Drilling of E1-I	Nov. 7, 2017	Nov. 15, 2017
Notching of E1-I	Nov. 16, 2017	Nov. 16, 2017
Drilling of E1-PDT	Nov. 28, 2017	Dec. 6, 2017
Drilling of E1-PDB	Dec. 6, 2017	Dec. 11, 2017
Drilling of E1-PSB	Dec. 11, 2017	Dec. 14, 2017
Drilling of E1-PST	Dec. 14, 2017	Dec. 21, 2107
Borehole geophysical logging	Jan. 08, 2018	Jan. 25, 2018
Well to natural fracture hydraulic connectivity survey	Feb. 2, 2018	Feb. 7, 2018
Installation of sensors in monitoring boreholes	Mar. 1, 2018	Mar. 22, 2018
Seismic characterization and ERT baseline imaging	Apr. 4, 2018	Apr. 19, 2018
Hydraulic Stimulation #1 at 142' Notch	May 21, 2018	May 22, 2018
Hydraulic Stimulation #2 at 164' Notch	May 22, 2018	May 24, 2018
Hydraulic Characterization #1 at 164' Notch	Jun. 14, 2018	Jul. 12, 2018
Hydraulic Stimulation #3 at 128' Notch	Jul. 18, 2018	Jul. 20, 2018
Hydraulic Characterization #2 at 164' Notch	Oct. 24, 2018	Nov. 20, 2018
Hydraulic Stimulation #4 at 142' Notch	Dec. 7, 2018	Dec. 20, 2018
Hydraulic Characterization #3 at 142' Notch	Dec. 21, 2018	Dec. 21, 2018

2.2 Hydraulic Stimulations

Four hydraulic stimulations were conducted, starting at the 142' Notch, then proceeding through the 164' and 128' Notches, and concluding with a second stimulation at the 142' Notch. Hydraulic characterization experiments were conducted twice at the 164' Notch and once at the 142' Notch. The overview in this section describes key events during the hydraulic stimulation and characterization experiments. The first hydraulic stimulation was conducted at the 142' Notch and was limited to an injection volume of 12 L. A hydraulic fracture was thought to have been created with a breakdown pressure of 31 MPa (4500 psi). A system leak during the shut-in period, precluded a complete analysis. The second hydraulic stimulation was conducted at the 164' Notch, over the course of three days, allowing for shut-in periods between injection stages. The first shut-in, after an injection of 2.1 L showed a classical response, and values for instantaneous shut-in pressure (ISIP), closure pressure, leakoff coefficient, and fracture toughness were generally as anticipated. An interpretation of the pressure decay during the second shut-in, after an additional injection of 23.5 L, suggested that the hydraulic fracture had intersected a natural fracture. This stimulation at the 164' notch was continued until an intersection with E1-OT was noted acoustically and flow occurred out of E1-P. A 2˚C temperature increase was additionally noted, at the point shown in Fig. 1a, in E1-OT, with the temperature rise occurring via the Joule-Thompson effect for water depressurization at the state conditions. Following a series of hydraulic characterization experiments at the 164' Notch, described in the following paragraph, an extended hydraulic stimulation experiment was conducted at the 128' Notch. The principal objective of this experiment was to create a hydraulic fracture between E1-I and E1-P, avoiding the OT-P connector fracture system. This hydraulic stimulation had difficulties with flow circumventing the inflatable packers. A hydraulic fracture was created, intersecting E1-OT, but not E1-P. After this stimulation, an additional set of hydraulic characterization experiments were conducted at the 164' Notch, and then a second stimulation experiment was completed at the 142' Notch. This hydraulic stimulation experiment involved high flow rates and pressures, and extended the hydraulic fracture beyond E1-P to E1-PDT, but not E1-PDB. Micro-seismic event locations (Schoenball et al., 2019) and the intersection of the hydraulic fracture with E1-PDT, and not E1-PDB, were evidence that the fracture extension tended upward toward the drift, as predicted by the modeling (White et al., 2018) of fracture growth under the stress gradient created by thermal cooling of the rock by the drift.

2.3 Hydraulic Characterizations

Three hydraulic characterization campaigns were conducted over the course of the year; two at the 164' Notch and one at the 142' Notch. For the first series of hydraulic characterization experiments at the 164' Notch, the principal objective was to quantify characteristics about the fracture system connecting E1-I and E1-P. A secondary objective was to improve the fraction of flow to E1-P. Prior to this experiment, the upper (i.e., closer to the collar) 6.1 m (20 ft) of the E1-OT borehole was grouted. All but the upper portion of the borehole was previously grouted upon installation of the sensors. The first experiment was a pressure transient test in both E1-I and E1-P at low flow rates (i.e., ≤ 20 ml/min). Peak pressures during these tests were below fracture propagation pressure at 18.1 MPa (2630 psi) for E1-I and 20.7 MPa (3000 psi) for E1-P. During both of these experiments, flows were noted from E1-OT and E1-PST, the latter of which indicated the connectivity of the OT-P connector beyond E1-P toward the drift. The second experiment was a series of step pressure injections in E1-I, during the first of these experiments flow from E1-P dropped sharply, with an associated rise in the flow from E1-PSB, potentially indicating that the hydraulic fracture was connected to the OT-P connector fracture system. The final experiment of the first series of hydraulic characterizations at the 164' notch involved high flow rates (i.e., up to 4 L/min) and pressures (i.e., 30.0 MPa or 4355 psi), which were above the fracture extension pressure. These high-flow rate experiments yielded maximum flows from E1-P of 0.4 L/min and E1-OT reaching 0.2 L/min, reaching 60% recovery at times. Flows from E1-PST and E1-PSB (i.e., 2.3 ml/min and 5.2 ml/min, respectively) did not show corresponding increases in rates, indicating the dynamic nature of the combined hydraulic and natural fracture system. The high-flow rate experiment concluded with the upward displacement of the packer and SIMFIP assembly in E1-I, with an associated buildup of pressure in the interval below the packer. This event provided evidence of the OT-P connector fracture system extending toward the bottom of E1-I.

The high-flow rate test at the 164' notch suggested the potential for a long-term circulation experiment, and the previous step-pressure experiments further suggested that an intermediate injection rate of 0.4 L/min would yield both circulation between E1-I and E1-P, at pressures below the fracture extension limit. The initiation of the intermediate-rate flow experiment required higher pressures than anticipated for the 0.4 L/min flow rate at 29.3 MPa (4250 psi). At the start of this experiment, water was flowing from E1-OT and from the collar of E1-P (i.e., from above the packed interval), with the packed interval set to span the anticipated hydraulic fracture. This was a strong indication that flow was preferentially entering E1-P via the OT-P connector fracture system over the hydraulic fracture. The inflatable packer string was moved up the E1-P borehole in three steps: 1) +1.2 m (+4 ft), 2) +1.8 m (+6 ft), and 3) +2.4 m (+8 ft). After the first two packer moves upward, no flow was observed out of E1-P, either from within or above the packed interval, but after the third move, flow was recorded from below the packed interval. Between the first and second packer assembly moves, the upper packer was deflated, and flow was observed from the E1-P collar, indicating the upper packer was covering the OT-P connector intersection. At this time, it became evident the importance of the natural fractures in understanding the hydraulic connections between E1-I and E1-P, and a common discrete fracture network campaign was started, which involved a re-examination of the cores and borehole logs, and creation of a catalog of natural fractures. The principal objective of this campaign was to develop a common conceptual model for the simulation teams of the combined hydraulic and natural fractures within Test Bed 1.

The second hydraulic characterization experiment was conducted from the 164' Notch in E1-I and was designed investigate the test bed sustained flow conditions, characterize the fracture network with electrical resistivity tomography (Johnson et al., 2019), and conduct a series of conservative and sorbing tracer experiments (Mattson et al., 2019). Prior to this experiment, the E1-OT borehole was sealed with epoxy to increase the flow resistance to the drift. To start the experiment injection flow rates were held at 0.4 L/min, and injection pressures held steady near 28.3 MPa (4100 psi). Under these steady flow conditions DNA and C-Dot tracers were injected and recovered. Flow was recorded from E1-P, below and within the packed interval, E1-OT, E1-OB, and E1-PST, and percent recoveries of the injected water approached 84%. During this time water was noticed flowing from bolts that anchor the wire mesh support structure of the drift, at the point labeled in Fig. 1b. Although the experiment was hampered with pump failures, backup pumps were available to maintain steady-

flow conditions. After roughly 7 days of injection at 0.4 L/min, the injection pressure started to increase, in spite of constant flow rate, and several attempts were made to halt the pressure rise by short-duration high-flow rate injections. Each of these pulses would result in a pressure drop with the resumption of injecting at 0.4 L/min, but then were followed by steady pressure increase at a rate of 115 kPa/hr (16.7 psi/hr). At this point the system was switched to a steady pressure injection at 29.0 MPa (4200 psi), which stabilized the pressure, but yielded reducing flow rates. To investigate whether scaling was causing the observed flow resistance, the injected water was switched to deionized and softened water, and bromine was added to the injection water in slugs to reduce biological fouling. About 1½ days after the switch to deionized water, the injection water chillers were switched on, and within 6 hours, the pressure dropped 1 MPa (150 psi) under a steady injection rate of 0.4 L/min. Pumping of chilled water was maintained, and after 90 hours of injection at 0.4 L/min the injection water temperature was 15.5˚C, the injection pressure was 28.4 MPa (4120 psi), and the percent recovery of injected water was 54%. After an additional 36 hours of pumping at 0.4 L/min, the pressure in the E1-I interval had increased to 29.0 MPa (4220 psi). After an additional 24 hours of steady-rate pumping, the injection pressure started to rise rapidly, with a concurrent drop in the recovery of water from the producing boreholes, which had principally become E1-OT. The injection pressure increased to 31 MPa (4500 psi), at which point the system was switched to pressure control, which resulted in a sharply falling injection rate, and following an additional 12 hours the system was shut down, and the second hydraulic characterization test was concluded.

The third characterization experiment was short termed and was conducted immediately after the hydraulic stimulation at the 142’ Notch. A principal objective of this characterization experiment was to locate fluid entry points in E1-P from the hydraulic stimulation in E1-I. A sewer camera was deployed for identifying the fluid entry points, so the hydraulic characterization was conducted without the inflatable packer string in E1-P, and the borehole was dewatered to just below the packer string location during the stimulation. The experiment started with a nominal flow rate of 0.4 L/min, which yielded an injection pressure of 22.8 MPa (3300 psi). Flows were observed from E1-OB and E1-P, and drips were noted coming from the drift ceiling, at the point along the drift noted in Fig. 1b, an indication that the hydraulic stimulation had extended the hydraulic fracture beyond E1-P and intersected the OT-P connector natural fracture system. The flow rate was increased to 2.0 L/min, yielding an injection pressure of 32.4 MPa (4700 psi), near the fracture extension pressure. Flows were observed from E1-OB, E1-P, E1-PST, and E1-PSB. The injection rate was increased to 4.0 L/min for two intervals of 70 and 22 minutes and in both cases the injection pressure showed only slight initial increases, followed by slowly decaying pressures, typical of fracture extension. Flow from E1-OB increased over the experiment from less than 0.01 to 0.4 L/min. The sewer camera logging in E1-P was able to identify six jetting points and one slit, which appeared to belong to two clusters, approximately 0.2 m (0.7 ft) apart, near the 30.5 m (100 ft) depth in E1-P. Whereas the mechanisms may be different, it should be noted that two clusters of jets, separated by a small distance, were also found in E1-P from the hydraulic stimulation at the 164’ Notch, and in both cases the location of the inflow to E1-P was near where one would predict based on the stress orientation.

3. MODELING HYDRAULIC STIMULATION WITHIN A FRACTURED DOMAIN

Pre-stimulation modeling and simulation results based on various approaches, e.g., cohesive zone finite element model (FEM), boundary element model (BEM), extended finite element model (xFEM) and discrete element model (DEM), all predicted the initiation and growth of more-or-less planar hydraulic fracture toward the production well. All these pre-stimulation modeling and simulations adopted the assumption of homogenous thermal and mechanical properties of the rock within the model domain of interest. While some modeling approaches like DEM incorporated random fluctuations of mechanical properties to represent small-scale heterogeneity, the rock within the domain of interest is statistically homogeneous at the scales beyond a few meters.

The actual stimulation experiments and data collected at the test bed, however, strongly indicate that the natural fractures and foliation structures of rocks that are widely presented within the test bed have significant influence on the initiation and growth of hydraulic fractures. The stimulation results indicate that the fracturing patterns at the test bed could involve both tensile opening of new cracks and shear-openings of natural fractures, which leads to very complicated fracturing patterns between the injection and production wells (~10 meters apart). One obvious challenge is to characterize the natural fractures between the wells at sufficiently high resolution and certainty, and in addition, their hydraulic and mechanical properties, and spatial connectivity. The hydraulic stimulation experiments also revealed an equally challenging difficulty of characterizing the size, shape and growth pattern of the hydraulic fracture itself.

To better understand the potential roles of natural factures on hydraulic fracture propagations within the test bed, the INL modeling team carried out preliminary 2D sensitivity study using a DEM model. Fig. 2 illustrates the 2D model domain setup with the presence of natural fractures and fracture clusters between the injection well and production well. While the natural fractures intersecting the wells can be determined from core logs, their spatial extensions away from the wellbores are unclear and not determined yet. We filled in the model domain with natural fractures in an arbitrary way, but based on the inferred statistics and patterns of fracture sets, orientations, sizes and fracture clusters using data obtained within and adjacent to the test bed. The rock matrix permeability (k_o) used in the sensitivity study is kept constant at 10^{-19} m^2. The rock tensile strength (T_o) is also kept constant at 5 MPa (725 psi) throughout all simulations. The typical rock tensile strength of rocks in the test bed ranges about ~3-5 MPa (~435-725 psi). The in-situ horizontal and minimum stresses are set to 21 and 31 MPa (3050 and 4500 psi), respectively, the same values as those used in pre-stimulation simulations.

Given the rock mechanical properties, in-situ stress condition, and spatial distributions of natural fractures, the most important input parameters for the model are the permeability and cohesive tensile strength of individual natural fractures. Site characterization efforts at the Collab test bed clearly indicate that those natural fractures exhibit a wide range of degrees of mineralization, from completely mineralized, to partially mineralized, to open (flowing) cracks. Generally, natural fractures were treated as “weak planes” in terms of mechanical strengths and “preferential” flow pathways in most numerical simulations. Therefore, in our 2D sensitivity study, we systematically decreased the mechanical cohesive strengths of natural fractures, while increased the permeability of natural fractures at the same time. Table 2 summarizes all initial sensitivity simulation scenarios. We started first by assuming the natural fractures have similar properties of the rock matrix, which essentially ignores the natural fractures (i.e., the pre-stimulation simulations). Then we

gradually increased the permeability of natural fractures with decreasing mechanical cohesive strength in the follow on simulation scenarios.

Simulated fracturing patterns in the initial 2D sensitivity studies are shown in Fig. 3, for the six simulation cases. It is worth mentioning in all sensitivity simulations, we explicitly put a natural fracture adjacent to the injection interval with the initial purpose to study the effect of a natural fracture on the fracture initiation process. In Case 1, all natural fractures have similar hydraulic and mechanical properties to the rock matrix (i.e., the modeled rock is statistically homogenous). A hydraulic fracture was initiated near the end of the injection interval, then gradually turned and propagated along the horizontal maximum stress direction. The small kinks and wavy fracture path are actually due to the local small scale random perturbations on rock shear/tensile strengths incorporated into the model. The fracturing is mainly tensile opening at the scale of the model domain. In Cases 2 and 3, the permeability of natural fractures was increased by 10 times with decreasing cohesive strength by 25%, the simulated fracturing patterns do not seem strongly affected by the presence of natural fractures, and we observe a single tensile hydraulic fracture that is largely directed by in-situ stress conditions. As we continue to increase the permeability of natural fractures by 100 times (i.e., Case 4, bottom-left figure) or decrease the cohesive strength of natural fractures by 50% (i.e., Case 5, bottom-middle figure), we still observe the propagations of a single tensile hydraulic fracture, in the direction largely dominated by in-situ stress conditions. However, the overall fracturing patterns start to become more complex. The fracture started to branch out along some natural fractures intersecting the main hydraulic fracture. We started to see opening along some natural fractures.

Table 2. Summary of sensitivity simulation scenarios defined by various combinations of permeability and mechanical cohesive tensile strength of natural fractures.

Simulation Case	**Permeability of natural fractures (relative to the rock matrix permeability K_0 of 10^{-19} m^2)**	**Mechanical cohesive tensile strength of natural fractures (relative to the rock matrix tensile strength T_0 of 5 MPa)**
1	$= k_o$	$= T_0$
2	$= 10^1 \times k_o$	$= T_0$
3	$= 10^1 \times k_o$	$= 0.75 \times T_0$
4	$= 10^2 \times k_o$	$= 0.75 \times T_0$
5	$= 10^1 \times k_o$	$= 0.5 \times T_0$
6	$= 10^4 \times k_o$	$= 0.1 \times T_0$

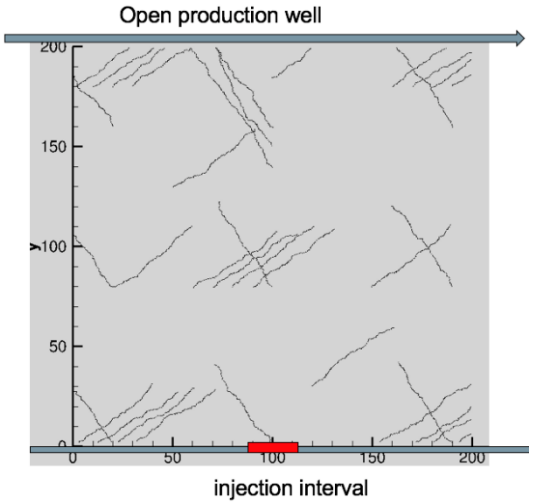

Figure 2: Illustration of the 2D model setup with the presence of natural fractures between the injection well (at the bottom) and open production well (at the top). The dimensionless distance of 200 in the Y direction corresponds to the dimensional distance of 10 meters between the wells.

In the more extreme case (i.e., Case 6, bottom-right figure), the permeability of natural fractures was increased by 4 orders of magnitude, and the cohesive strength was decreased by 90%, representing poorly mineralized, and permeable natural fractures with an equivalent hydraulic aperture on the order of 0.1 micron. In this case, the fracturing is almost completely dominated by opening of natural fractures. Once the natural fractures were pressured, we also observe multiple tensile openings from the tips of natural fracture, which was strongly affected by the in-situ stress conditions. However, all these tensile-opened fractures would be arrested by natural fractures if they intersect with natural fractures. The combined openings of natural fractures, multiple tensile opening fractures from the tips of pressurized natural fractures, and propagation arresting together generated very complex fracturing pattern in the simulation, which poses significant challenge to characterize them in the field with sufficient certainty and resolution. Also, of interest in this particular case is that a continuous flow path toward the injection well beyond the injection interval was established during the continuous injection. This possibly explains the field observation of the bottom hole pressure build up below the packer during one of the stimulation experiments, as the team is quite confident about the sealing performance of the packers during injection. This initial 2D sensitivity study clearly reveals the

importance of incorporating effects of natural fractures into numerical model predictions in order to provide realistic and reliable model predictions on fracturing patterns and stimulated rock volume. The EGS Collab team has been actively developing 3D DFN models of natural fractures for the Collab test bed. We also expect the 3D hydraulic fracturing simulations with natural fractures could yield more complicated fracturing behaviors.

4. MIXED-MODE, TORTUOSITY DOMINATED, AND NATURAL FRACTURE NETWORKS

During the design stages for EGS Collab Experiment 1, the team from The University of Oklahoma (OU), applied their GeoFrac2D model to study possible fracture trace angles at the wellbore, and utilized the GeoFrac3D computer code for two borehole orientations; vertical and horizontal in the direction of σ_h. In considering the experimental results from the Hydraulic Stimulation #2 at 164' Notch, the OU has approached the problem of understanding the hydraulic connection between the injector, E1-I, and producers, E1-P and E1-OT, via three modeling approaches: 1) mixed-mode fracturing, 2) tortuosity dominated hydraulic fracturing, and 3) hydraulic completion via extensions of natural fractures. The objective for the mixed-mode fracturing modeling was to understand the deviations in the stimulation pressure history from what would be expected for classical pure hydraulic fracturing. The OU team addressed this modeling with a two-dimensional simulation that considered three different initial hydraulic fracture orientations within a stress domain with existing natural fractures, develop by Ankush Singh and Mark Zoback, from Stanford University (Ankush et al, 2019). These simulations were initialized with either a single hydraulic fracture perpendicular to the borehole, a single fracture angled to the borehole, or a pair of fractures perpendicular to the borehole. Mode 1 fracture propagation was assumed and when the hydraulic fracture intersected a natural fracture, the natural fracture undergoes pressurization and potentially slip, and is assumed to only extend at the fracture tip (i.e., flaws along the fracture length are ignored). The tip from which extension occurs depends on the stress distribution around the tip, which depends on the stress shadows from other natural fractures. Natural fractures impact the pressure profile depending on how they are orientated with σ_h. As the hydraulic fracture intersects a natural fracture, pressure drops and as pumping continues the pressure increases to a level sufficient to extend the natural fracture along σ_h, yielding a variable pressure profile.

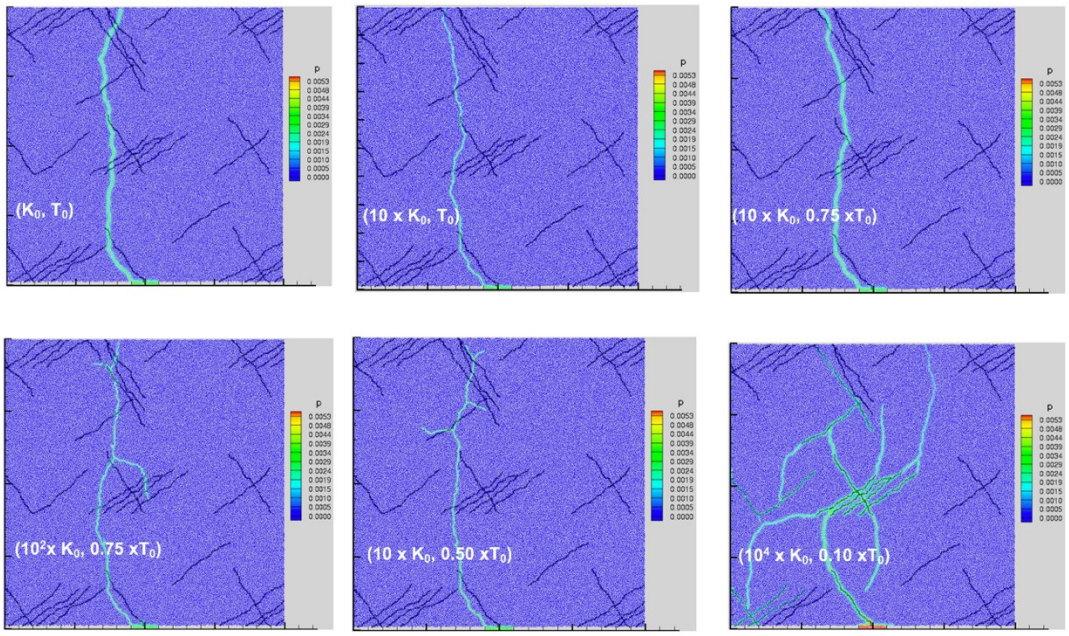

Figure 3: Simulated fracturing patterns under various combinations of the permeability and cohesive strength of natural fractures.

Another explanation for the pressure perturbations that occurred during Hydraulic Stimulation #2 at 164' Notch, is one of tortuosity friction within the hydraulic fracture near the borehole, with the remainder of the hydraulic fracture being planar-like. Simulations of hydraulic fracture propagation were executed and compared against the net pressure from the experimental results; where net pressure is the difference between injection pressure and fracture extension pressure. Fracturing was assumed to occur orthogonal to σ_h. Values for σ_h, Young's modulus, Poisson's ratio, pore pressure, and matrix permeability were held constant, with the fracture toughness allowed to serve as a fitting parameter. Agreement in net pressure between the numerical simulations and experimental observations was achieved with a fracture toughness of 6.0 MPa $m^{1/2}$. A second simulation was executed that assumed the stimulated fracture was a natural fracture, oriented such that the normal stress would be greater than that for the hydraulic fracture. The agreement in net pressure between the numerical simulation and experimental observations were poorer than those for the hydraulic fracture simulation, with the fit for the fracture toughness being a value of 4.0 MPa $m^{1/2}$. This result supports the notion of a hydraulic fracture being generated from E1-I, with near-borehole tortuosity having a critical role in defining the pressure drop from injector to producers.

In the third simulation suite, a network of natural fractures was taken from the common discrete fracture network developed from the examination of borehole cores, borehole visual and geophysical logs, and geological examination of the drift. The initial fracture network

is shown in Fig. 4a; where fractures are labeled by their intersection points with boreholes and the depth in feet down the borehole. For example, natural fracture PDB-130, intersects borehole E1-PDB at a borehole depth of 130 ft from the collar. Interestingly the initial fracture network does not yield a hydraulic connection between E1-I and E1-P. In these simulations, natural fractures are assumed to propagate only along their plane, as fracture cohesion is exceeded, and the initial fracture radii were between 3.2 to 5.3 m. With water injection the natural fractures extend to radii of 4.58 to 6.83 m, and complete a hydraulic connection between E1-I and E1-P, through a series of intermediate fractures, some of which comprise the OT-P connector fractures. Fracture extension was modeled via an analytical solution within the toughness dominated regime. This work collectively demonstrates the potential for three distinct conceptual models and associated numerical solutions providing an explanation for the Hydraulic Stimulation at 164' Notch, with agreement with the experimental data.

5. TRACER BREAKTHROUGH

During the design stages of the EGS Collab Experiment 1, a series of simulations were executed that were directed at forecasting the duration of the tracer and thermal circulation experiments. The principal experiment design objectives were to minimize the circulation time required to see tracer and temperature breakthroughs at E1-P, without circulating at flowrates that would extend fractures. The LLNL team estimated achievable circulation rates for two scenarios: 1) assuming homogeneous in situ stress distribution and an idealized penny-shaped fracture, and 2) assuming a heterogeneous stress field and a somewhat irregular fracture shape. Using its GEOS code (Settgast et al. 2017; Fu et al., 2013), the LLNL team demonstrated that the highest flow that could be achieved across the fracture without incurring continued fracture propagation was achieved when the back-pressure is slightly lower than σ_h for the homogeneous stress field. For the heterogeneous stress field, the simulations show that the maximum achievable circulation rate without continuing to propagate the fracture is likely below 0.6 L/min. When spatial variation of stress is significant, there exists the risk of the production wellbore encountering the fracture at a high stress region and the circulation rate might be one order of magnitude lower than the maximum value. With an upper circulation rate established, circulation duration for thermal breakthrough was modeled by LLNL and NREL/CSM teams. Low, moderate and high circulation rates were modeled using an idealized penny-shaped fracture with constant aperture. At low anticipated rates below 0.6 L/min, these idealized models indicate months or years are required to achieve a 1°C drop in produced fluid temperature. Thermal breakthrough is delayed due to a conduction-dominated mode of thermal decline at rates below 0.6 L/min. In addition to thermal breakthrough, the NREL/CSM team modeled conservative tracer response at multiple circulation rates below 0.6 L/min, and these idealized models indicate produced tracer concentrations peak within 2 hours following the start of slug injection. In summary, at rates below 0.6 L/min idealized models predict rapid conservative tracer response; however, a conduction-dominated mode of thermal decline severely delays thermal breakthrough.

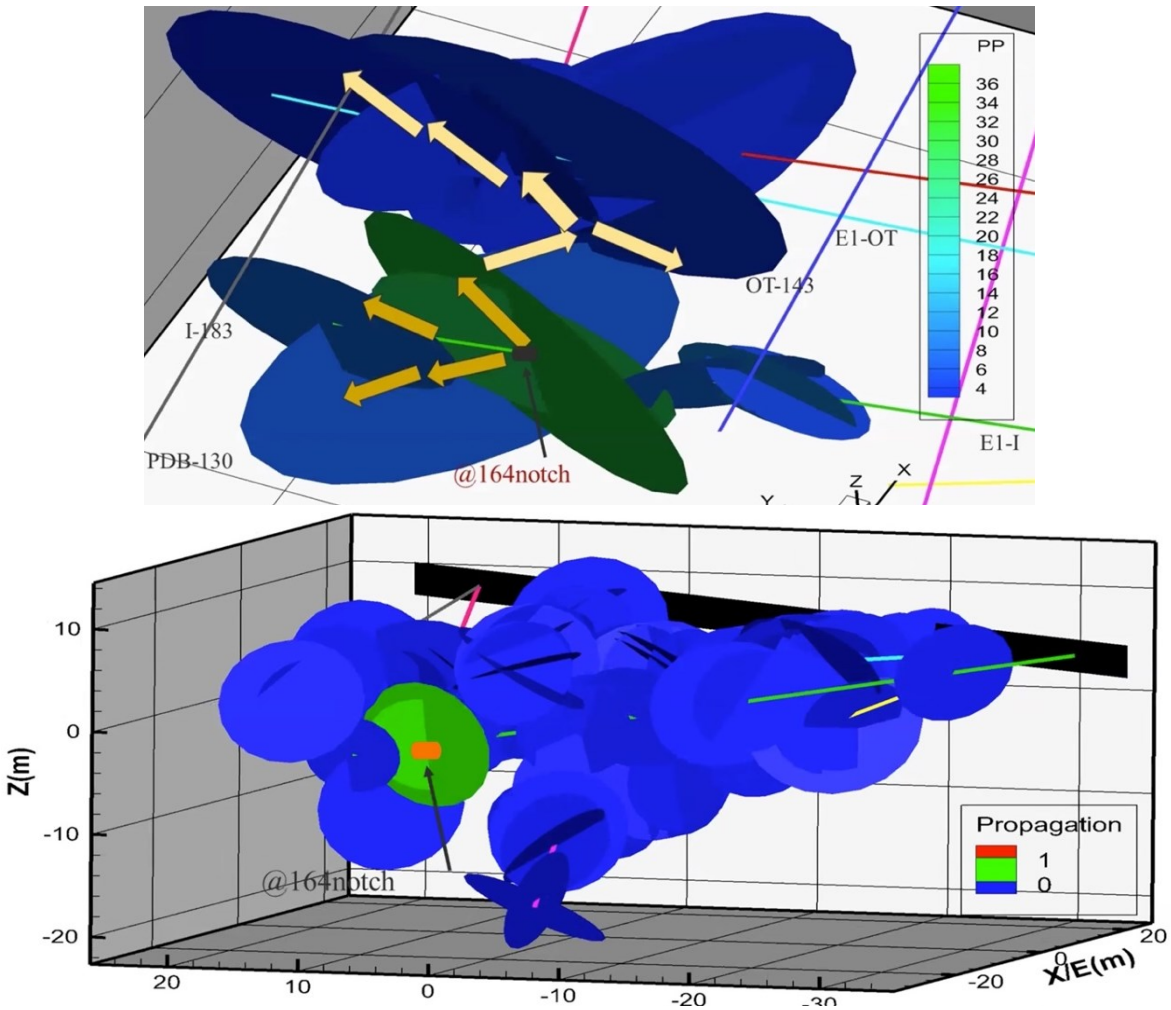

Figure 4: (a) Initial fracture network with two natural fractures shown in green near the 164' Notch in E1-I. (b) Final state of fracture network after stimulation. Images generated with Leapfrog Software

During the Hydraulic Characterization #2 at 164' Notch a series of conservative (i.e., non-sorbing) tracer experiments were conducted using 6 distinct DNA tracers (Zhang et al., 2017) were injected at different combinations on Oct. 24, Oct. 25, Oct. 31 and Nov. 1, 2018, and C-Dots (Mattson et al., 2019), on Oct. 26, 31, Nov. 1, Nov. 7, and Nov. 8, 2018. The first three C-Dots tracer experiments were conducted after E1-OT had been repaired and the later two were conducted after a series of high pressure and high flow rate stages that re-opened flow from E1-OT. The tracer recovery plots from these four experiments were used by the LLNL team to characterize a conceptual model of the fracture system, comprising one hydraulic and one natural fracture, between the injector E1-I and producers E1-P below the packed interval (E1-Pbottom), E1-P within the packed interval (E1-Pinterval), and E1-OT (Wu et al., 2019a). The conceptual model of the fracture system comprises one hydraulic fracture, which connects E1-I with E1-OT, E1Pbottom, E1-PDB, and E1-PDT, and intersects the natural fracture, as shown in Fig. 5a. The natural fracture is aligned with the conceptual model for the OT-P connector fracture, intersects E1-Pinterval, E1-PSB, and E1-PST, is shown in Fig. 5b. Simulations were executed with a recently developed tracer transport solver developed within GEOS, a LLNL developed geomechanics simulator (Wu et al., 2019b), via a sequential approach, where flow and transport through the hydraulic fracture were solved, driven by fluid injection, fluid loss to the environment, fluid produced at the connected boreholes, and fluid transferred to the natural fracture. In the second step, flow and transport through the natural fracture is simulated, driven by fluid transferred from the hydraulic fracture, fluid lost to the environment, and fluid produced at the connected boreholes. Both fractures were modeled as either having a uniform aperture or heterogeneous aperture. Under uniform aperture conditions, the hydraulic fracture had eight adjustable parameters: fracture extents A_1 and A_2; aperture w; diffusion coefficient D_f, natural fracture transfer parameters q_i, P_1, and P_2, and fluid lost to the environment parameters θ, and L, as shown in Fig. 5a. The natural fracture has three adjustable parameters: aperture w′, and fluid lost to the environment parameters θ′, and L′, as shown in Fig. 5b. For heterogenous fractures the parameters are mean aperture, aperture standard deviation, and correlation length.

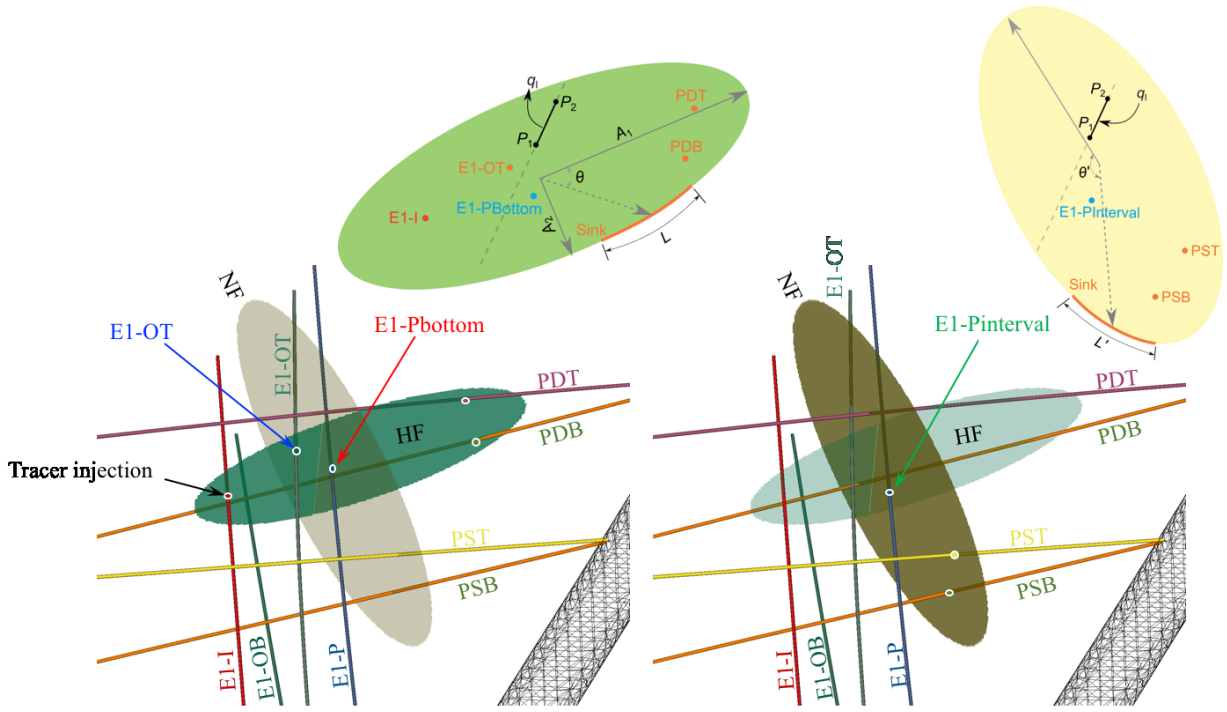

Figure 5: (a) Connections of the hydraulic fracture (b) connections of the natural fracture.

Tracer recovery curves from E1-OT and E1-Pbottom, taken on Oct. 1, were used as benchmarks for determining the hydraulic fracture parameters. A brute-force Monte Carlo approach was taken over the parameter space, for the uniform aperture scenario, with 2 million realizations executed. Results that showed the best agreement with the experimental tracer recoveries were identified and commonalities in parameters were recorded among the top fits. For the hydraulic fracture, the key commonalities were that fluid leaked to the environment from a sink to the west and a uniform aperture of roughly 100 microns was likely. For the natural fracture, 0.8 million realizations were executed over the uniform aperture parameters space. Unlike the hydraulic fracture, however, the natural fracture failed to show good agreement with the tracer recoveries, taken on Oct. 1, from E1-Pinterval, using a uniform aperture model. The simulations were then repeated over 0.8 million realizations, but with a heterogenous aperture, and scenarios were identified that showed agreement with the tracer recoveries in E1-Pinterval. The same modeling approach was used for tracer recoveries, taken on Nov. 1, 7, and 8, and differences in the hydraulic and natural fractures were identified between the periods before and after the high pressure and high flow rate stages.

High performance computing allows scientist and engineers to tackle problems with computational domains with hundreds of millions of unknowns solved simultaneously. Combined with the scripting languages, high performance computing additionally allows the solution of moderately sized problems, such as the hydraulic and natural fracture systems described in this section, over millions of realizations. The workflow for a single realization in this work involved four steps: 1) generating a random parameter set, 2) generating an aperture realization from the parameter set, 3) converting the realization into an input file for GEOS, and 4) comparing the simulation output against the tracer recoveries, as shown in Fig. 6. Whereas this workflow would be a reasonable undertaking for a single realization without the aid of scripts and high performance computing, it would impossible for millions of realizations. The sorting of realizations by goodness of fit over millions of realizations, additionally requires scripting to make the execution tractable. The result from this approach is conceptual model of the fracture network connecting E1-I with the producing boreholes, that honors the experimental data. The novel aspect of this modeling approach is the ability to extract key findings from the results, such as the natural fracture having an aperture ten times larger than the hydraulic fracture, and that the flow in the hydraulic fracture is more disperse, whereas in the natural fractures is more channelized.

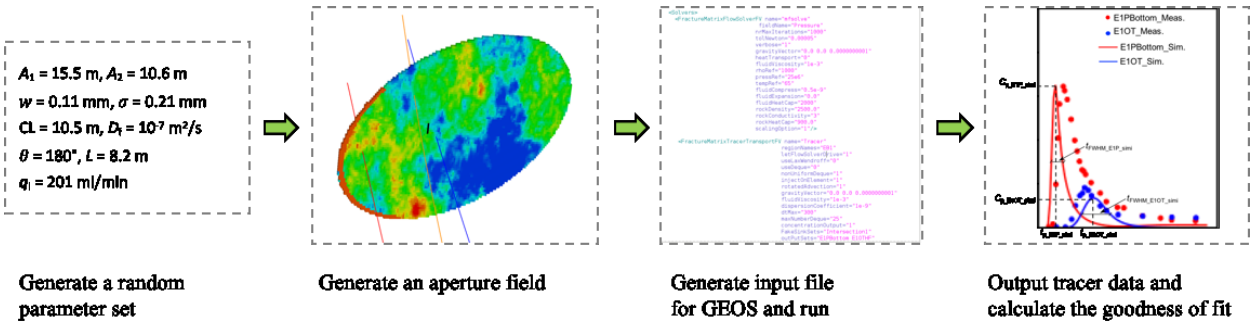

Fig. 6: Workflow for a single realization of the brute-force Monte Carlo simulation scheme, which involves iterating over the single realization workflow hundreds of thousands of times.

6. THERMAL ENVIRONMENT SURROUNDING THE DRIFT

The test bed for Experiment 1 of the EGS Collab project is on the western flank of the West Access Drift on the 4850 Level. Ambient temperatures at the 4850 Level, determined from Homestake mine surveys, were estimated to be 34˚C. Drifting activities started at the 4850 Level in 1949 and a variety of active cooling systems were used to reduce working temperatures for the miners. Gold mining operations ceased in Homestake mine in 2001 and the dewatering pumps were switched off in 2003. In 2007 the National Science Foundation approved the Deep Underground Science and Engineering Laboratory (DUSEL), which sought to establish an interim research facility at the 4850 Level and ultimately a deeper facility at the 8000 Level. With the establishment of DUSEL and then later the Sanford Underground Research Facility (SURF) dewatering pumps were switched on, and the water level in the mine reached the 4850 Level on May 13, 2009 (Dobson and Salve, 2009). Ventilation supplied from the Yates and Ross shafts serve to cool the open mine workings. The temperature profiles surrounding the 4850 Level drift are a function of the early mining activities from 1949 through 2003, the mine closure from 2003 to 2009, and then the reopening of the 4850 Level for scientific and engineering research from 2009 to present. Prior to the drilling of the eight experimental boreholes, three teams made estimates of the temperature profiles in the test bed, using temperature measurements taken during the underground reconnaissance for the DUSEL facility (Dobson and Salve, 2009) and during the EGS-Collab project within the kISMET boreholes (Oldenburg et al., 2016; Roggenthen and King, 2017) were used for verification of the numerical simulation results. Teams from INL, LBNL, and PNNL developed solutions for temperature profiles around the 4850 Level. Although the modeling teams took different approaches to the problem, the simulation results were in good agreement between the groups and with the measurements from the kISMET boreholes (White et al., 2018).

After completion of the eight boreholes, shown in Fig. 1, temperature logs were recorded. A comparison of the temperature profile within the experimental test bed from the borehole logging and simulation predictions is shown in Fig. 7a. In this figure the isosurfaces of temperature are profiles generated from the numerical simulation and the color-scaled lines are the temperatures measured from the borehole logs. The agreement between the borehole temperature measurements and numerical simulations results are good. Calibrated distributed temperature sensor (DTS) measurements were also taken in the monitoring boreholes, nearly continuously throughout the experimental period. Numerical simulations indicate that the drift cooling should yield a radial temperature distribution around the drift, approaching the depth dependent ambient temperature around a radius of 50 m away from the drift centerline. Plots of the temperatures in the boreholes from the thermistor temperature logs, the calibrated DTS measurement on May 1, 2018, and the kISMET logs are shown versus radial distance from the drift centerline in Fig. 7b. The numerical simulation results closely match the kISMET logs. Boreholes E1-PST and E1-PDT do not show the expected characteristic shape of a radial temperature distribution, indicating something other than thermal conduction is impacting the temperature along these boreholes. The geophysical logging of the boreholes occurred within a month of the completion of the borehole drilling, and the drilling fluid was water available through the mine utility, generally at temperatures between 20 to 25˚C. During the logging campaign flows from E1-PSB and E1-PST were noted, with flows from E1-PST being generally ten times that of E1-PSB. The original conceptual model of the thermal environment surrounding the drift was one based on the thermal conduction being the principal heat transport mechanism between the rock and drift, with advection and evaporation having a role at the rock-drift contact. This comparison makes it apparent that natural fractures and fluid flow has an impact the test bed temperature field.

7. THERMAL SIGNATURES

A fundamental reason for developing and applying numerical simulators is to provide scientists and engineers with better understanding of physical systems. A modeling exercise was completed by the LBNL team that investigated heat transfer and temperature change of the water flowing from an injection borehole to a production borehole through an idealized radial fracture (Zhang et al., 2018). The principal objective of the numerical study was to forecast the thermal breakthrough time for various scenarios of initial temperature distributions, fracture apertures, and pressure differentials. An unexpected outcome of the study was the prediction that a small temperature increase would be observed at the production borehole prior to the arrival of the thermal signature from injection well, as shown in Fig. 8a. Further investigation into this outcome led to the realization that water at the pressure and temperature conditions anticipated for the experimental conditions of the test bed, had a negative Joule-Thomson coefficient. A negative Joule-Thomson coefficient indicates that temperature increases with decreasing pressure during an isenthalpic process. Uncertainty about this effect led to a short laboratory experiment that verified the direction and magnitude of temperature change during a pressure drop. Most of the hydraulic stimulation and characterization experiments conducted in the test bed have been done without back pressure on the production borehole, E1-P, which has yielded large pressure drops across the interface between the fracture and production borehole, as noted by the observed jetting fluid from the E1-P

borehole walls. Fluid entering E1-OT, however, has experienced both small and large pressure drops across the borehole wall, depending on the nature of the flow resistance between the point of fracture intersection and the drift. Under situations where E1-OT contributed a considerable fraction of the produced flow the thermal signature at the entry point was about 2˚C above the ambient temperature, as shown in Fig. 8b, during the Hydraulic Simulation #2 at the 164' Notch. For water flowing from high to low pressure under isenthalpic conditions, the expected temperature increase is 0.22 C/MPa, which would suggest at pressure drop of at least 9 MPa between the hydraulic fracture and E1-OT. The impact of thermal gradient around the drift, as shown in Fig. 7a, on produced water temperature was small but visible over a wide portion of the fracture plane.

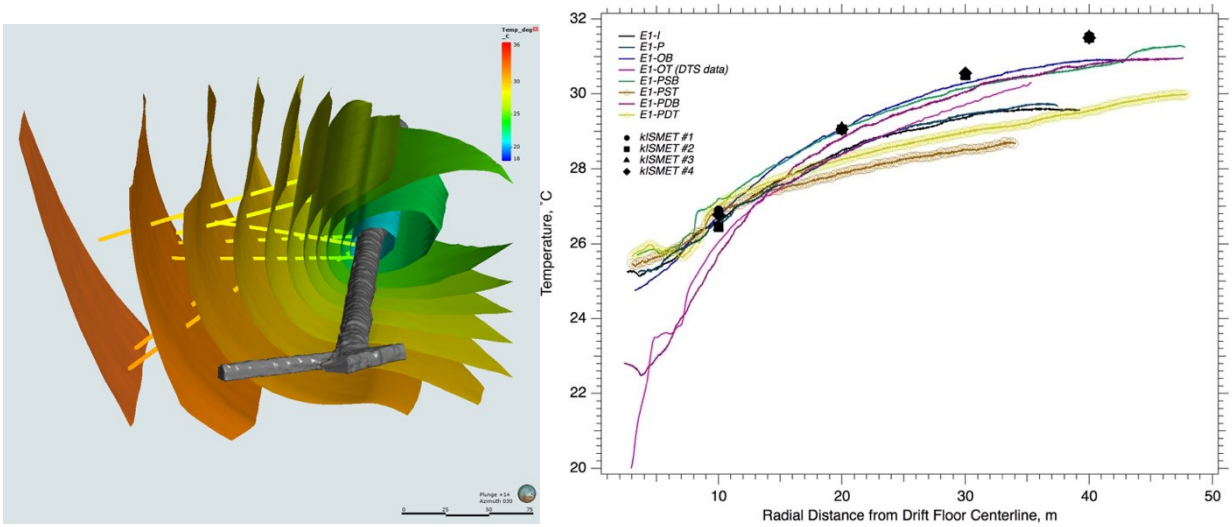

Figure 7: (a) Comparison of temperature profiles within the test bed volume from numerical simulations and temperature logging of the boreholes. Image generated with Leapfrog Software. (b) comparison of temperature profiles as a function of radial distance from the drift centerline, including kISMET boreholes.

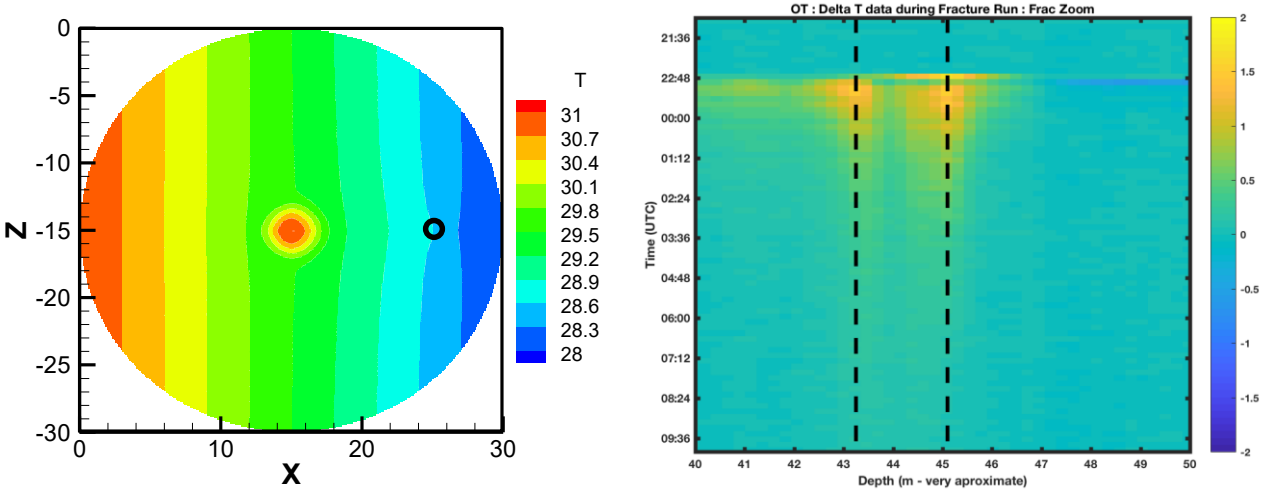

Figure 8: (a) Numerical simulation results for the temperature increase around a production well for fluid injection in a planar fracture, (b) Distributed temperature sensor (DTS) response at E1-OT on May 26.

8. ELECTRICAL RESISTIVITY TOMOGRAPHY

The six monitoring boreholes within the Experiment 1 test bed, (i.e., E1-OB, E1-OT, E1-PSB, E1-PST, E1-PDB, and E1-PDT) each contain 16 electrodes grouted in place, comprising an array of electrodes surrounding the expected hydraulic fracture zone, primarily in the region bounded by boreholes E1-PST, E1-PSB, E1-PDT and E1-PDB. These electrodes enable characterization of the three-dimensional (3D) low-frequency electrical properties of the phyllite rock, and changes in those properties in response to hydraulic stimulation, circulation of chilled water, and injection of water with contrasting electrical conductivity to the ambient formation water, using both static and time-lapse Electrical Resistivity Tomography (ERT). The ability of ERT and associated challenges in imaging fractured rock systems using a 3D cross-borehole configuration was previously demonstrated at a limestone quarry (Robinson et al., 2015). Baseline imaging, conducted prior to hydraulic stimulation and characterization activities in the test bed, revealed a highly heterogeneous rock fabric, ranging over four orders of magnitude in bulk electrical conductivity, and high polarization capacity. Baseline imaging results are consistent with borehole logs and core studies. Electrical conductivity is governed by rock mineralogy, primary and secondary porosity,

saturation, and fluid conductivity within the host rock, all of which are important sources of information concerning stimulation and flow behavior. Ideally, ERT imaging is conducted in regions free from artifact-inducing anthropogenic sources of noise or metallic infrastructure. To protect against rock fall, the 4850 level is outfitted with continuous steel mesh that is rock-bolted to the drift wall (see Fig. 9). Additionally, packer systems deployed in injection and production intervals are operated using a series of stainless steel tubes. The mesh and steel tubing respectively form equipotential surfaces and lines during ERT current injections. Both synthetic modeling and raw data collected during packer installations confirmed that the mesh and tubing have a significant influence on the ERT data.

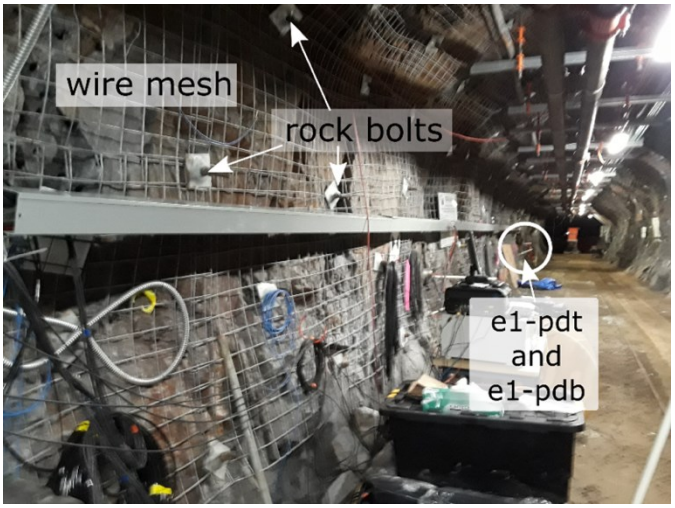

Figure 9: Wire mesh and rock bolts on the drift wall constitute a continuous electrical conductor that forms an equipotential surface during ERT current injections. Stainless steel tubing connected to packers in the injection and production wells (not shown) form an equipotential line during ERT current injections.

To address the influence of the mesh and tubing, each was explicitly simulated during the forward modeling phases of the ERT inversion using the method of Johnson and Wellman (2015). Comparisons of the ERT inversion results with and without infrastructure forward modeling prior to stimulating the 164.24 ft notch are shown in Fig. 10a and Fig. 10b, respectively (Johnson et al, 2019). Fig. 10b exhibits a significant improvement in image coherence and reveals that the Experiment 1 test bed exists within a folded and dipping structure of repeating high and low conductivity layers in the upper margin, with relatively massive, high conductivity structure in the lower margins. These results are consistent with rock fabric and fracture patterns extracted from detailed analysis of oriented borehole logs.

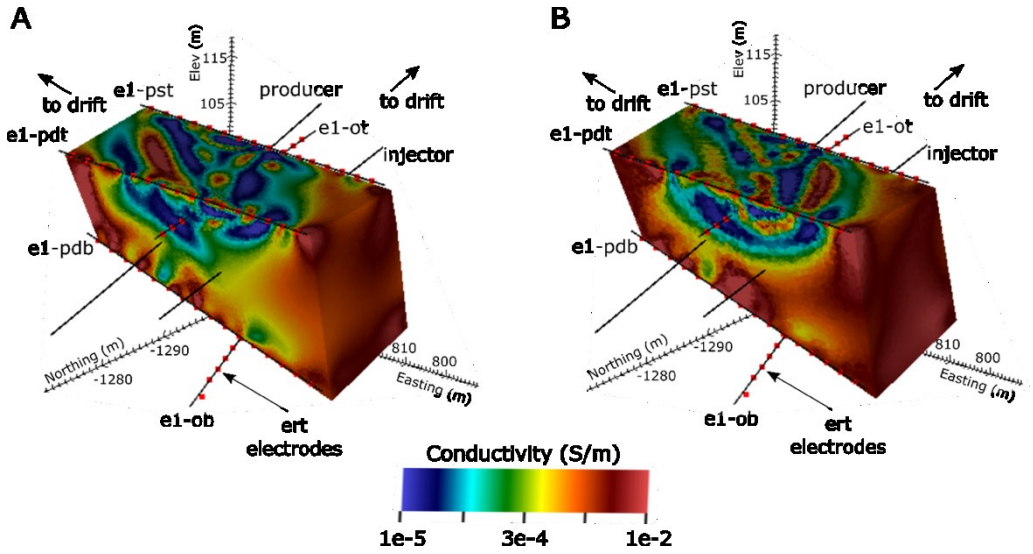

Figure 10: Baseline ERT inversion results without (A) and with (B) modeling of the equipotential surfaces on the drift wall and equipotential lines within the injection and production boreholes. Inversion (B) reveals a folded and dipping sequence of conductive and resistive layers highly consistent with rock fabric and fracture patterns determined from core logs.

9. DISCRETE FRACTURE MODELING

To support modeling and simulation studies for the EGS Collab project, researchers at Virginia Tech are developing a synthetic mesh representation of the fractured rock volume for Experiment 1. This effort implements the TOUGH3 numerical simulation code (Jung et

al., 2017) to study the potential for thermodynamic processes to influence the thermal breakthrough signature at Experiment 1. While previous research successfully implemented TOUGH3 for simulating fluid flow in discrete two-dimensional fracture networks (Gierzynski and Pollyea, 2017), embedding discrete fractures in a three-dimensional rock volume introduces unique challenges because it is well known that coarse grid discretization can introduce errors in the numerical solution, particularly for heat transfer from wall rock into the flowing fracture. To overcome this challenge, the research team is reproducing the Experiment 1 discrete fracture network (DFN) model (Fig. 11a) as a three-dimensional unstructured grid using the recently developed TOUGH2 plugin for the LaGrit library of mesh generation tools (Sentís and Gable, 2017). In this approach, each fracture (and borehole) is embedded in the rock volume as a gridded object with finite geometry and the surrounding grid cells are systematically coarsened into the wall rock. To maintain near-orthogonal grid cell connections, the conceptual model is discretized by Voronoi tessellation. This approach leverages recent advances in parallel computing for both mesh generation and high-fidelity, multi-physics numerical simulation with TOUGH3.

The National Renewable Energy Laboratory and Colorado School of Mines (NREL/CSM) team is modeling tracer response measured during EGS Collab circulation experiments. This team is using a coupled thermal, hydrological, mechanical, and chemical simulator (TOUGH2-CSM). Recent enhancements made to TOUGH2-CSM (Winterfeld et al., 2019) include the addition of tracers to a TOUGH2 (Pruess et al., 2012) property module, the capability to model sorbing tracers, and an embedded fracture formulation. Current models include hydraulic fractures and natural fracture networks with variable apertures. These models have replicated measured tracer response, and thermal breakthrough simulations are being run to assist in the design of planned thermal circulation experiments.

The STOMP-GT numerical simulator (White and Oostrom, 2006) was originally developed for analyzing nuclear waste repositories where the geologic system comprised partially saturated conditions within a highly fractured tuffaceous rock and the engineered system comprised sealed canisters that released heat to the host rock from radioactive decay. To model these kinds of coupled geologic and engineered systems, the simulator solves coupled equations for multiphase flow, heat transport, and reactive transport, in an equivalent continuum geologic medium. As noted above the STOMP-GT simulator was used to estimate the temperature distribution within Test Bed 1, but was not truly capable of modeling fractured systems, beyond those with a few discrete fractures or those which were considered highly fractured. To model discrete fracture networks, under the influence of dynamic geomechanical stress, with thermal and hydrologic coupling to the rock matrix, engineers at PNNL are developing an embedded fracture modeling capability in STOMP-GT. The first step in this development has been the creation of a porothermoelastic geomechanics module (GEOMech) for the simulator, and the second has been the development of embedded fracture modeling capabilities. When completed the simulator will be capable of modeling the tracer and thermal circulation experiments of the EGS Collab project. An example of a preliminary simulation of tracer transport across an embedded fracture with transfer to the rock matrix is shown in Fig. 11b, where the fracture aperture was unique for each triangular fracture grid cell. The team is currently developing flow and transport algorithms for fracture-fracture intersections. As with the Virginia Tech team, the PNNL team recognizes the challenges of modeling the coupling of fracture and matrix systems, and is currently using a transfer function approach.

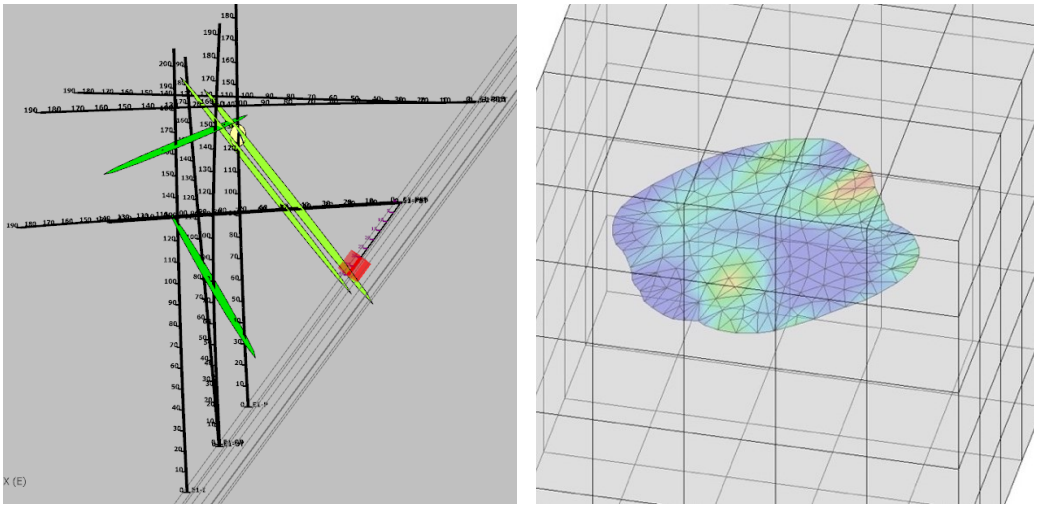

Figure 11: (a) Conceptual model of natural fracture network created from hydraulic connections observed during the hydraulic stimulations, based on DTS anomalies and drift observations. Red cylinder is the location of inflow on the drift wall from extended injection. Image generated with FracMan Software (Golder Associates, Inc.). (b) Embedded fracture within a hexahedral discretization of the rock matrix, showing color-scaled tracer concentration during a hydraulic circulation scenario (injection and production wells not shown).

10. CONCLUSIONS

The EGS Collab project investigates hydraulic stimulation and circulation processes at the meso-scale under near *in-situ* stress conditions for commercial enhanced geothermal fields, and the United States Department of Energy, Geothermal Technologies Office's (GTO) new field-scale EGS research facility, the Frontier Observatory for Research in Geothermal Energy (FORGE). During the design stages of the first experiment of the project, whose principal objective was to create a hydraulic fracture between an injection and production borehole, numerical simulation played an important role in answering critical questions about the experimental elements; such as, borehole

orientations, anticipated seismicity, circulation conditions that avoid fracture propagation, protections provided by production boreholes on fracture propagation, thermally altered stress states, and breakthrough times for tracer and thermal experiments. The teams and numerical simulation codes applied to answer these design questions are those that are internationally recognized, undergoing extensive verification, and are high performance computing capable, and were able to answer a suite of design questions. Prior to drilling the eight experiment boreholes and conducting hydraulic stimulations, the numerical simulation process carried out during the design stages, required an iterative process of conceptualization and verification via numerical simulation. This process was implemented through the evolution of the design, starting with the simple question of borehole orientation, through understanding the impact of fracture propagation on the altered stress state in the experimental volume caused by drift excavation, ventilation, and dewatering. Numerical simulators applied to answer experimental design questions were varied numerical approaches and development teams, but overall yielded equivalent understandings of the fracturing and circulation processes, and generally showed good quantitative agreement.

At first inspection, the creation of a 10-m hydraulic fracture between two boreholes in phyllite rock that had foliation characteristics on two dimensional scales, but otherwise appeared to have a low natural fracture density, seemed straightforward, especially given the available knowledge about the stress state from the nearby kISMET experiments. During the drilling of the eight experiment boreholes, natural fractures were noted during logging, with some of those fractures showing extensions that spanned multiple boreholes. Moreover, what became known as the OT-P connector natural fracture system, yielded flow at near-zero pressures between E1-OT and E1-P during the drilling of E1-P. After the series of hydraulic stimulation and hydraulic characterization experiments conducted in Test Bed 1, the EGS Collab team has discovered the critical importance of the near-vertical natural fractures that transect the experimental volume. The response being the development of a common discrete fracture network (CDFN), and an iteration in the modeling and simulation teams' approach to conducting simulations. The development of a CDFN involved a second detailed inspection of the borehole cores, sewer camera borehole logs, and geologic inspections of the drift; plus, the incorporation of these data into a hydrostructural model via the FracMan software. On the numerical side, the response has been to explore innovative approaches to using existing numerical tools, develop new capabilities for legacy simulators, or bring other existing software into play. For geothermal and subsurface numerists, this is often the nature of the work; applying computer codes to better understand a system, and then retooling when the system is different than expected. Whereas, the EGS Collab team has learned much about Test Bed 1, there remain unanswered questions about the extent of the natural fractures and their connectivity, and the current extent of the hydraulic fractures at all three notch locations. As in the design stages, numerical simulation, with our recent advances in approaches and capabilities, will aid in the more complete understanding of the experimental system.

ACKNOWLEDGMENTS:

This material was based upon work supported by the U.S. Department of Energy, Office of Energy Efficiency and Renewable Energy (EERE), Office of Technology Development, Geothermal Technologies Office, under Award Number DE-AC05-76RL01830 with PNNL. The United States Government retains, and the publisher, by accepting the article for publication, acknowledges that the United States Government retains a non-exclusive, paid-up, irrevocable, world-wide license to publish or reproduce the published form of this manuscript, or allow others to do so, for United States Government purposes. The research supporting this work took place in whole or in part at the Sanford Underground Research Facility in Lead, South Dakota. The assistance of the Sanford Underground Research Facility and its personnel in providing physical access and general logistical and technical support is acknowledged, with a special recognition to George Vandine for his dedication to this project and safe guidance underground. Where noted, figures in this paper were generated using Leapfrog Software. Copyright ©Seequent Limited. Leapfrog and all other Seequent Limited product or service names are registered trademarks or trademarks of Seequent Limited. The Simulation and Modeling Working Group recognizes the Field and Discrete Fracture Network Working Group team members for their long hours in the field, quite often nearly a mile underground. Without their efforts, dedication, and creativity the data that forms the basis of our numerical simulations would simply not exist.

REFERENCES

Dobson, P.F., and Salve, R.: *Underground Reconnaissance and Environmental Monitoring Related to Geologic CO_2 Sequestration Studies at the DUSEL Facility, Homestake Mine, South Dakota*, LBNL-2858E, Lawrence Berkeley National Laboratory, Berkeley, CA (2009).

Fu, P., Johnson, S.M., and Carrigan, C.R.: An explicitly coupled hydro-geomechanical model for simulating hydraulic fracturing in complex discrete fracture networks. *International Journal for Numerical and Analytical Methods in Geomechanics*, 34(14): 2278-2300 (2103).

Gierzynski, A.O., Pollyea, R.M.: Three-phase CO_2 flow in a basalt fracture network, *Water Resources Research*, 53(11):8980-8989 (2017).

Johnson, T.C., Wellman, D.C.: Accurate modeling and inversion of electrical resistivity data in the presence of metallic infrastructure with known location and dimension." *Geophysical Journal International*, 202(2):1096-1108, doi:10.1093/gji/ggv206 (2015).

Johnson, T.C., Strickland, C., Vermeul, V., Mattson, E., Knox, H.A., Ajo-Franklin, J., Schwering, P.C., Kneafsey, T.J., and Blankenship, D., EGS Collab Team: EGS Collab Project Electrical Resistivity Tomography Characterization and Monitoring. *Proceedings*, 44rd Workshop on Geothermal Reservoir Engineering, Stanford University, Stanford, CA, SGP-TR-214 (2019).

Jung, Y., Pau, G.S.H., Finsterle, S., Pollyea, R.M.: TOUGH3: A new efficient version of the TOUGH suite of multiphase flow and transport simulators, *Computers & Geosciences*, 108:2-7 (2017).

Kneafsey, T.J., Dobson, P.F., Ajo-Franklin, J.B., Valladao, C., Blankenship, D.A., Knox, H.A., Schwering, P., Morris, J.P., Smith, M., White, M.D., Johnson, T., Podgorney, R., Mattson, E., Neupane, G., Roggenthen, W., and Doe, T.: The EGS Collab Project: Stimulation and Simulation, *Proceedings,* 52nd U.S. Rock Mechanics/Geomechanics Symposium, ARMA-2018-1345 (2018).

Knox, H., Fu, P., Morris, J., Guglielmi, Y., Vermeul, V., Ajo-Franklin, J., Strickland, C., Johnson, T., Cook, P., Herrick, C., Lee, M., Bauer, S.J., Baumgartner, T., Blankenship, D., Bonneville, A., Boyd, L., Brown, S.T., Burghardt, J.A., Carroll, S.A.: Fracture and Flow Designs for the Collab/SIGMA-V Project, *Proceedings*, Geothermal Resources Council 41st Annual Meeting, Salt Lake City, Utah (2017).

Mattson, E., Zhang, Y., Hawkins, A., Johnson, T., Ajo-Franklin, J., Neupane, G., EGS Collab Team: Preliminary Collab Fracture Characterization Results from Flow and Tracer Testing Efforts. *Proceedings*, 44rd Workshop on Geothermal Reservoir Engineering, Stanford University, Stanford, CA, SGP-TR-214 (2019).

Morris, J.P., Fu, P., Dobson, P., Ajo-Franklin, J., Kneafsey, T.J., Knox, H., Blankenship, D., White, M.D., Burghardt, J., Doe, T., EGS Collab Team: Experimental Design of Hydrofracturing and Fluid Flow at the DOE EGS Collab Testbed, *Proceedings*, 52nd U.S. Rock Mechanics/Geomechanics Symposium, ARMA-2018-007 (2018).

Nolte, K.G.: Principles for Fracture Design Based on Pressure Analysis, Society of Petroleum Engineers, SPE-10911-PA, https://doi.org/10.2118/10911-Pa, (1988).

Oldenburg, C.M., Dobson, P.F., Wu, Y., Cook, P.J., Kneafsey, T.J., Nakagawa, S., Ulrich, C., Siler, D.L., Guglielmi, Y., Ajo-Franklin, J., Rutqvist, J., Daley, T.M., Birkholzer, J.T., Wang, H., Lord, N.E., Haimson, B.C., Sone, H., Vigilante, P., Roggenthen, W.M., Doe, T.W., Lee, M.Y., Ingraham, M., Huang, H., Mattson, E.D., Zhou, J., Johnson, T.J., Zoback, M.D., Morris, J.P., White J.A., Johnson, P.A., Coblentz, D.D., and Heise, J..: *Intermediate-Scale Hydraulic Fracturing in a Deep Mine, kISMET Project Summary 2016*, LBNL-1006444, Lawrence Berkeley National Laboratory, Berkeley, CA (2016).

Pruess, K., Oldenburg, C., Moridis, C.: *TOUGH2 User's Guide, Version 2.1*, Report LBNL-43134, Lawrence Berkeley National Laboratory, Berkeley, Calif. (2012).

Robinson, J., Johnson, T., Slater, L.: Challenges and opportunities for fractured rock imaging using 3D cross-borehole electrical resistivity. *Geophysics*, 80(2):E49-E61, https://doi.org/10.1190/geo2014-0138.1, (2015).

Roggenthen, W.M., and King, D.K.: Quick Review of T data for kISMET Area (5/19/17), *Unpublished EGS Collab Project Report*, Lawrence Berkeley National Laboratory, Berkeley, CA (2017).

Schoenball, M., Ajo-Franklin, J., Blankenship, D., Cook, P., Dobson, P., Fu, P., Gugliemi, Y., Kneafsey, T., Knox, H., Neupane, G.H., Petrov, P. Robertson, M., Schwering, P., Templeton, D., Ulrich, C., Wood, T., The EGS Collab Team: Microseismic Monitoring of Meso-scale Stimulations for the DOE EGS Collab Project at the Sanford Underground Research Facility, *Proceedings*, 44rd Workshop on Geothermal Reservoir Engineering, Stanford University, Stanford, CA, SGP-TR-214 (2019).

Sentis, M.L., Gable, C.W.: Coupling LaGrit unstructured mesh generation and model setup with TOUGH2 flow and transport: A case study. Computers & Geosciences, 108:42-49 (2017).

Settgast, R.R, Fu, P., Walsh, S.D.C, White, J.A., Annavarapu, C., and Ryerson, F.J.: A Fully Coupled Method for Massively Parallel Simulation of Hydraulically Driven Fractures in 3-Dimensions. *International Journal for Numerical and Analytical Methods in Geomechanics*, 41(5): 627-653, (2017).

Singh, A., Neupane, G.H., Zoback, M., Dobson., Ulrich, C., Schwering, P.C., Roggenthen, W., Uzunlar, N., Doe, T., Johnston, B, EGS Collab Team.: Slip Tendency Analysis of Fracture Networks to Determine Suitability of Candidate Testbeds for the EGS Collab Hydroshear Experiment. *Proceedings*, 44rd Workshop on Geothermal Reservoir Engineering, Stanford University, Stanford, CA, SGP-TR-214 (2019).

White, MD and M Oostrom.: *STOMP Subsurface Transport Over Multiple Phases, Version 4.0, User's Guide,* PNNL-15782 (2006).

White, M.D., Fu, P., Huang, H., Ghassemi, A., EGS Collab Team: The Role of Numerical Simulation in the Design of Stimulation and Circulation Experiments for the EGS Collab Project, *Proceedings*, GRC Transactions, Vol. 41 (2017).

White, M.D., Fu, P., Ghassemi, A., Huang, H., Rutqvist, J., Johnston, B., EGS Collab Team: Numerical Simulation Applications in the Design of EGS Collab Experiment 1, *PROCEEDINGS, 44th Workshop on Geothermal Reservoir Engineering*, Stanford University, Stanford, CA (2018).

Winterfeld, P., Johnston, B., Beckers, K., Wu, Y.-S.: Code Modifications for Modeling Chemical Tracers and Embedded Natural Fractures at EGS Collab. *Proceedings*, 44rd Workshop on Geothermal Reservoir Engineering, Stanford University, Stanford, CA, SGP-TR-214 (2019).

Wu, H., Fu, P., Morris, J.P., Mattson, E.D., Hawkins, A.J., Zhang, Y., Settgast, R.R., Ryerson, F.J., EGS Collab Team: Characterizing fracture flow in EGS Collab experiment based on stochastic modeling of tracer recovery, *Proceedings*, 44rd Workshop on Geothermal Reservoir Engineering, Stanford University, Stanford, CA, SGP-TR-214 (2019a).

Wu, H., Fu, P., Morris, J.P., Settgast, R.R., Ryerson, F.J., EGS Collab Team: A numerical scheme to reduce numerical diffusion for advection-dispersion modeling: Validation and application, *Proceedings*, 44rd Workshop on Geothermal Reservoir Engineering, Stanford University, Stanford, CA, SGP-TR-214 (2019b).

Zhang, Y., Zeng, Z., Li, K., Horne, R.N.: DNA Barcoding for Fractured Reservoir Analysis – An Initial Investigation, *Proceedings*, 42nd Workshop on Geothermal Reservoir Engineering Stanford University, Stanford, California, February 13-15, SGP-TR-212 (2017).

Zhang, Y., Doughty, C., Pan, L., Kneafsey, T.: What Could We See at the Production Well Before the Thermal Breakthrough, *PROCEEDINGS, 44th Workshop on Geothermal Reservoir Engineering*, Stanford University, Stanford, CA, SGP-TR-213 (2018).